NOTES AND CORRESPONDENCE

A Nonlinear Baroclinic Wave-Mean Oscillation with Multiple Normal Mode Instabilities

R. M. SAMELSON AND C. L. WOLFE

College of Oceanic and Atmospheric Sciences, Oregon State University, Corvallis, Oregon

29 August 2002 and 16 October 2002

ABSTRACT

An unstable, nonlinear baroclinic wave-mean oscillation is found in a strongly supercritical quasigeostrophic f-plane numerical channel model with 3840 Fourier components. The growth of linear disturbances to this time-periodic oscillation is analyzed by computing time-dependent normal modes (Floquet vectors). Two different Newton–Picard methods are used to compute the unstable solution, the first based on direct computation of a large set of Floquet vectors, and the second based on an efficient iterative solver. Three different growing normal modes are found, which modify the wave structure of the wave-mean oscillation in two essentially different ways. The dynamics of the instabilities are qualitatively similar to the baroclinic dynamics of the wave-mean oscillation. The results provide an example of time-dependent normal mode instability of a strongly nonlinear time-dependent baroclinic flow.

1. Introduction

Baroclinic instability, and disturbance growth in baroclinic flows, are fascinating physical processes with fundamental importance for numerical weather prediction. Instabilities of steady zonal flows have been studied extensively since the pioneering investigations of Charney (1947) and Eady (1949), but relatively less attention has been paid to instabilities of time-dependent flows.

One approach to this latter problem is to consider time-periodic flows. This approach offers a framework for investigating the behavior of disturbances to time-dependent flows, which is intermediate between the study of disturbances to steady flows and disturbances to flows with general time dependence (e.g., Joly and Thorpe 1991; Farrell and Ioannou 1996). Time-periodic flows present many of the same technical and conceptual obstacles as flows with more general time dependence, but their disturbance growth properties are amenable to quantitative analysis in terms of time-dependent normal modes. A number of recent studies have examined periodic solutions of geophysical fluid models and their stability (Jiang et al. 1995; Itoh and Kimoto 1996; Jiang and Ghil 1997; Kazantsev 1998, 2001; Fantini and Davolio 2001; Samelson and Tziperman 2001).

Perhaps the simplest existing physical model of midlatitude baroclinic dynamics is the Phillips (1954) two-layer quasigeostrophic model of baroclinic instability. Samelson (2001, 2002) has identified and analyzed unstable time-periodic baroclinic wave-mean oscillations in this model for the weakly nonlinear limit of marginal supercriticality (Pedlosky 1971; Pedlosky and Frenzen 1980). Strongly unstable flows in this model have been previously studied numerically by Klein and Pedlosky (1986). Here, we extend these previous numerical studies to identify an unstable, strongly nonlinear, time-periodic, baroclinic wave-mean oscillation for the most strongly supercritical parameter values considered by Klein and Pedlosky (1986). The phase–space dimension of the numerical model is 3840, necessitating the use of special techniques to locate the oscillation and compute its stability.

The physical model is briefly reviewed in section 2. Section 3 describes the unstable oscillation, and sections 4 and 5 discuss the corresponding Floquet and singular vector analyses, respectively. The results are summarized in section 6.

2. Model

a. Formulation

The model studied here is a two-layer, f-plane, quasigeostrophic fluid in a periodic channel with a rigid lid

Corresponding author address: Dr. R. M. Samelson, College of Oceanic and Atmospheric Sciences, 104 Ocean Admin Bldg., Oregon State University, Corvallis, OR 97331-5503.
E-mail: rsamelson@coas.oregonstate.edu

at the upper boundary, and Ekman dissipation at both upper and lower boundaries. The mean layer depths are equal, and the standard no-normal-flow boundary conditions are imposed at the channel walls along $y = \{0, 1\}$. The equations are

$$Q_{jt} + J(\Psi_j, Q_j) = -r\nabla^2\Psi_j, \qquad j = 1, 2, \quad (2.1)$$

where Ψ_j and Q_j are the streamfunction and potential vorticity, respectively, in layer j, $j = 1, 2$, and $\nabla^2 = \partial^2/\partial x^2 + \partial^2/\partial y^2$. The upper- and lower-layer ($j = 1$ and $j = 2$, respectively) streamfunctions may be conveniently written as the sum of a constant mean shear and an arbitrary function:

$$\Psi_1(x, y, t) = -\frac{1}{2}U_s y + \psi_1(x, y, t), \quad (2.2)$$

$$\Psi_2(x, y, t) = +\frac{1}{2}U_s y + \psi_2(x, y, t). \quad (2.3)$$

The potential vorticities are

$$Q_1(x, y, t) = \nabla^2\Psi_1 - F(\Psi_1 - \Psi_2), \quad (2.4)$$

$$Q_2(x, y, t) = \nabla^2\Psi_2 - F(\Psi_2 - \Psi_1). \quad (2.5)$$

Here, U_s is the vertical shear of the steady zonal flow solution $\psi_1 = \psi_2 = 0$, and r is the Ekman damping coefficient.

The wave-mean oscillation discussed below is a solution of these nonlinear equations for the parameters $U_s = 1$, $r = 0.474\,342$, $F = 55.769\,60$, the most strongly supercritical set of parameter values considered in the numerical study by Klein and Pedlosky (1986). In the scaled notation of this latter study, which extended previous work on the weakly nonlinear problem for marginally supercritical shear, the corresponding parameter values are $\gamma = 0.2$, $\Delta = 45$. For these parameter values, the steady zonal flow $\psi_1 = \psi_2 = 0$ is linearly unstable to six normal modes, and nonlinear numerical solutions show chaotic behavior (Klein and Pedlosky 1986).

Small disturbances to the wave-mean oscillation will satisfy a linearized form of (2.1), in which the periodic wave-mean oscillation is the flow about which the equations are linearized. Once the periodic solution is known, the solutions of the corresponding linearized equations may be computed by standard techniques for linear differential systems with periodic coefficients (e.g., Coddington and Levinson 1955), referred to here as Floquet theory. For a periodic orbit solution, any linear disturbance may be written as a fixed sum of the Floquet eigenvectors $\{\phi^j(t), j = 1, 2, \ldots, N\}$, where each vector has the form $\phi^j(x, y, t) = \Phi^j(x, y, t) \exp(\lambda_j t)$, for a function $\Phi^j(x, y, t)$, with $\Phi^j(x, y, t + T) = \Phi^j(x, y, t)$ [or possibly $\Phi^j(x, y, t + T) = -\Phi^j(x, y, t)$]. In general, the functions ϕ^j and Φ^j and the characteristic exponents λ_j may be complex; also, the eigenvalue spectrum may include a continuous component (see, e.g., Brevdo and Bridges 1997), and the time dependence may include a polynomial component, if the corresponding eigenvalue has multiplicity greater than one. The modes considered here turn out to have real distinct λ_j and so also real ϕ^j and Φ^j. Modes with (in general, real parts of) λ_j positive grow exponentially, and correspond to time-dependent normal mode instabilities of the oscillation. Each ϕ^j is a solution of the linearized equations about the oscillation and, as written, represents both the upper- and lower-layer components of the disturbance. The Floquet problems were solved numerically using two different Newton–Picard methods, as described next. The reader uninterested in the technical aspects of these computations may skip this description.

b. Newton–Picard solution

As discussed in detail below, the periodic wave-mean oscillation identified here in a chaotic regime is linearly unstable, as it must be: if it were instead stable, nearby solutions would approach it as a limit cycle, rather than remain chaotic. Since it is unstable, essentially all nearby solutions eventually diverge from it as time evolves, and special techniques are necessary to compute the periodic solution. The basic method used here is a multidimensional Newton–Picard iteration. The number of unstable modes is small compared to the total phase–space dimension of the two-layer system, which for 48 $\times$ 40 horizontal spectral resolution is 3840, and this can be exploited by computing the Newton iteration in a small subspace that contains the unstable modes. Convergence in the orthogonal, much larger subspace is achieved simply by forward (Picard) integration, in the same way that forward integration of the full equations would lead to convergence toward a limit cycle if no unstable modes existed. The combined Newton–Picard iteration can be much more efficient than a full Newton's method, because of the large reduction in the dimension of the space in which the Newton's method is carried out. The technical obstacle to this approach, of course, is that the subspaces depend on the solution, and are not known beforehand.

We computed the periodic solution described here in several steps. First, a long time series from a chaotic numerical solution was examined to locate an approximately periodic segment. This segment was sufficiently close to periodic that a preliminary Floquet vector normal mode analysis was possible. The preliminary Floquet analysis used a direct approach: the linear evolution during the cycle of a set of independent initial disturbances was computed, and the Floquet vectors and characteristic multipliers obtained by solving the corresponding eigenvalue problem. Because of the large dimension of the system and the length of the cycle, the sets of initial disturbances used here were not complete, consisting of 120 to 2880 members, compared to the 3840 required for completeness. This procedure nonetheless gave interesting and useful preliminary results, including accurate values for the leading Floquet mode

growth rates, even for the most severe of these truncations.

The approximately periodic solution was then used as an initial guess for a Newton–Picard iteration scheme. This scheme used an explicit Newton's method on the fixed subspace defined by the 12 leading modes from the preliminary Floquet vector analysis, and Picard iteration on the complement of this fixed subspace. Approximate Floquet vectors were then obtained directly for this solution, by computing the linear evolution of a set of independent initial disturbances formed from the 24 along-channel and 10 across-channel gravest modes, and solving the corresponding Floquet eigenvalue problem.

To refine the improved estimate of the periodic solution, a version of the Newton–Picard solver PDECONT (Lust et al. 1998) was then implemented. In the configuration used here, this solver computes the leading Floquet vectors iteratively, following an approach that is related to well-known numerical schemes for computing Lyapunov vectors (Shimada and Nagashima 1979; Benettin et al. 1980) or growing normal modes (e.g., Samelson and Pedlosky 1990) by time stepping and rescaling, but with the addition of sophisticated subspace iteration and locking algorithms. The solver also optimizes the calculations needed for the Newton step, avoiding matrix inversions and other demanding computations that would otherwise be required. Consequently, the needed Floquet vector estimates can be efficiently updated at each iteration, accelerating the convergence of this second Newton–Picard scheme dramatically relative to the first.

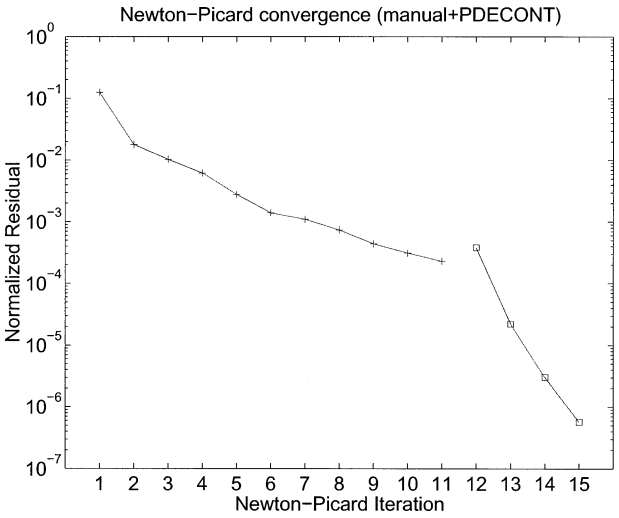

FIG. 1. Relative difference between initial and final states of the numerical solution for the unstable, nonlinear, wave-mean oscillation vs iteration step for the manual (+, steps 1–11) and PDECONT (□, steps 12–15) Newton–Picard implementations.

3. Nonlinear wave-mean oscillation

As described in the previous section, two Newton–Picard schemes were used successively to compute the unstable periodic solution. Eleven steps of the first Newton–Picard scheme were sufficient to reduce the relative difference in the initial and final states from more than 10^{-1} to less than 10^{-3}, and thus to indicate that the iteration was converging toward a true periodic solution (Fig. 1). The second Newton–Picard iteration, using the PDECONT solver, was halted after four steps, which decreased the relative difference in the initial and final states to less than 10^{-6}, providing practical confirmation of convergence (Fig. 1).

The solution obtained by this second iteration is the baroclinic wave-mean cycle analyzed and presented here (Fig. 2). The cycle is a strongly nonlinear analog of the weakly nonlinear wave-mean oscillation whose dynamics and stability were analyzed by Samelson (2001, 2002). Its qualitative characteristics are similar to the weakly nonlinear cycle. It consists of a periodic wave-mean oscillation, involving growth and decay of a nonlinear wave whose dominant structure is the gravest along-channel and across-channel Fourier component. There are two wave growth and decay events during each cycle, with the second offset from the first by half the channel length. The period of the PDECONT solution is $T = 38.484\ 57$, very close to the first Newton–Picard estimate $T = 38.485$. The streamfunction evolution summarized in this section is essentially indistinguishable for the two Newton–Picard solutions.

Each of these wave growth and decay events begins with a nearly zonal flow, modified by a perturbation whose dominant structure is the gravest along-channel and across-channel Fourier component (Fig. 2a; $t = 0/50$). This perturbation has the characteristic westward phase shift with height of a baroclinically unstable disturbance, and rapidly grows to finite amplitude (Fig. 2a; $t/T = 10/50$). When the perturbation reaches maximum amplitude, there are closed contours around both the high and low pressure cells, and the phase shift and the zonal-mean vertical shear of the zonal flow near the center of the channel both decrease substantially (Fig. 2a; $t/T = 13/50$). The phase shift then reverses, the disturbance decays, and the vertical shear of the zonal flow is re-established (Fig. 2a; $t/T = 16/50, 19/50$). Finally, the flow returns to near zonal, exactly as before the onset of wave growth, but with the perturbation shifted zonally by half the channel length, and the cycle repeats.

A decomposition of the streamfunctions into barotropic ($\psi_B = \psi_1 + \psi_2$) and baroclinic ($\psi_T = \psi_1 - \psi_2$) components reveals the development, during the wave growth phase, of stationary barotropic circulations that advect heat (proportional to ψ_T) downgradient, across the channel (Fig. 2b; $t/T = 0/50, 10/50, 13/50$). During the wave decay phase, the weakening barotropic circulations advect some of this heat back across the channel and up the gradient, extracting energy from the wave and re-establishing the baroclinic zonal flow (Fig. 2b; $t/T = 16/50, 19/50, 25/50$).

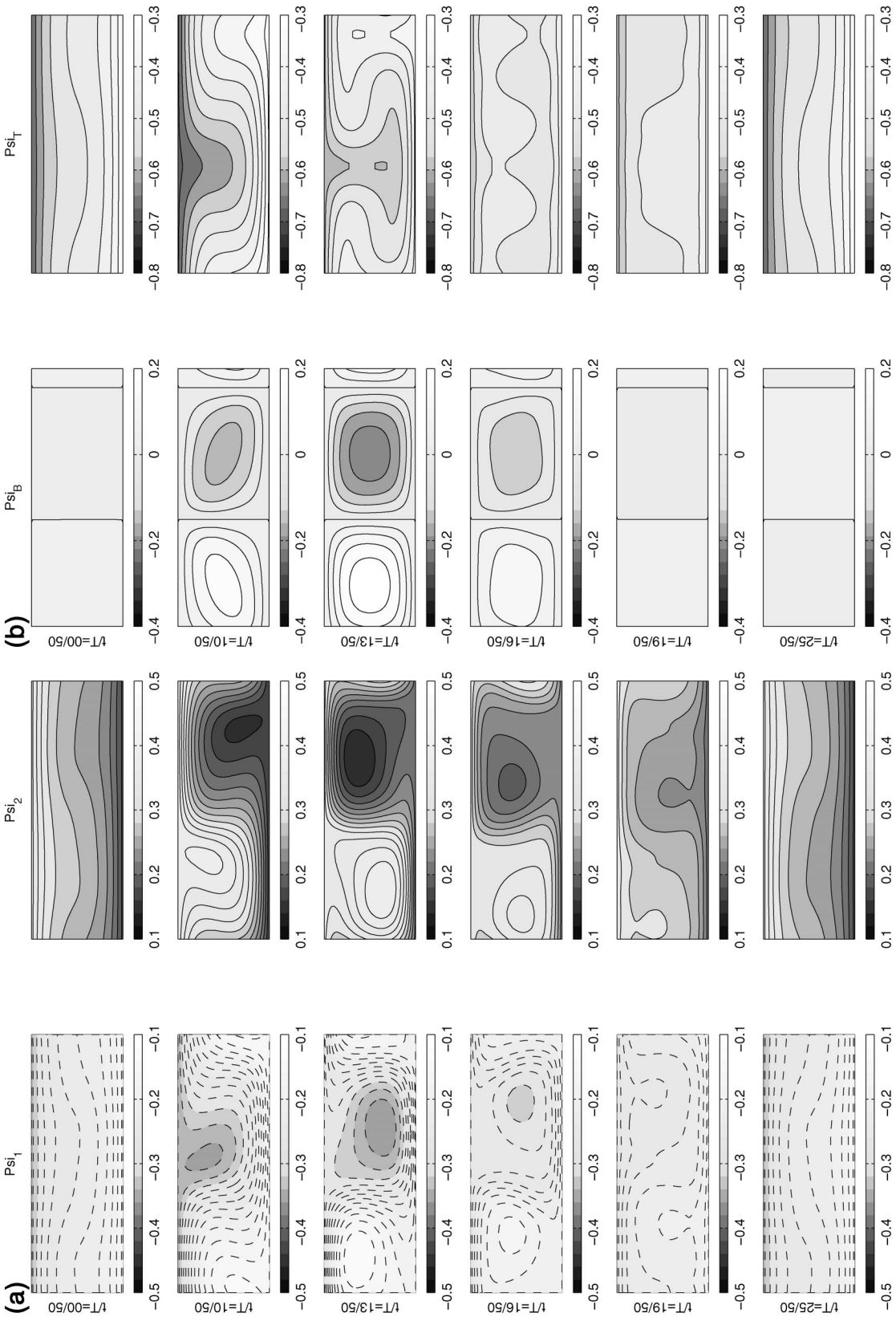

FIG. 2. (a) Contours of upper- (lhs) and lower-layer (rhs) streamfunctions vs x (horizontal axes) and y (vertical axes) during the evolution of the unstable, nonlinear, wave-mean oscillation. (b) Contours of barotropic (lhs) and baroclinic (rhs) streamfunctions vs x (horizontal axes) and y (vertical axes) during the evolution of the unstable, nonlinear, wave-mean oscillation.

4. Time-dependent normal mode instabilities

The Floquet vectors are the normal modes for linear disturbances on the unstable cycle. Two different estimates of the leading Floquet modes are available from the Newton–Picard solutions discussed above. The first method provided estimates of the first several hundred leading Floquet exponents and vectors, while the second provided results only for the first 7 leading modes, since only these were required by the efficient, iterative PDECONT solver. The accuracy of the vectors was checked in each case by integrating the Floquet vector disturbances over one cycle, and comparing the initial and final conditions. When scaled by the corresponding Floquet multiplier, these should be identical. The first 12 vectors from the first Newton–Picard solution and the first 5 vectors from the refined, PDECONT solution satisfied this criterion to an acceptable numerical accuracy. Only these vectors are considered here. Evidently, the remaining vectors failed to satisfy this criterion because of inaccuracies resulting from the incompleteness of the set of initial disturbances, which neglected many high along-channel and cross-channel Fourier components, or because of other related numerical effects induced by spectral truncation in the explicit linearization of the spectral model. Work is in progress to address this issue in related computations, on which we will report elsewhere. Here, we will focus primarily on the characteristics of the growing and neutral modes, for which accurate results were obtained for both Newton–Picard solutions. The plots of the Floquet vectors discussed in this section were obtained by the direct method, using 2880 independent initial disturbances, corresponding to the gravest 36 along-channel modes and all 40 cross-channel modes.

Both methods yielded three growing ($\lambda_j > 0$, $j = 1$, 2, 3) modes and one neutral ($\lambda_4 = 0$) mode (Fig. 3). The remaining modes were all damped. The values of the four leading Floquet exponents from the two different methods agreed to within less than 0.1%. Modes 5–7 showed slightly greater differences, up to roughly 1%; note that the PDECONT algorithm is not designed to provide accurate estimates of damped modes.

The corresponding Floquet structure functions Φ^j were computed by initializing the linearized equations with the corresponding eigenvector from the Floquet analysis, integrating the equations forward for one oscillation period, and normalizing the results at each time by the exponential growth factor $\exp(\lambda_j t)$. Mode 4, the neutral mode, is proportional to the time derivative of the wave-mean cycle. Consequently, its dynamics reflect the same baroclinic instability processes that maintain the wave-mean cycle, and its physical structure is dominated by the same gravest Fourier components that characterize the wave-mean cycle (Fig. 4). Some smaller-scale features appear in the mode-4 streamfunction fields at certain times during the cycle, such as at $t/T = 13/50$.

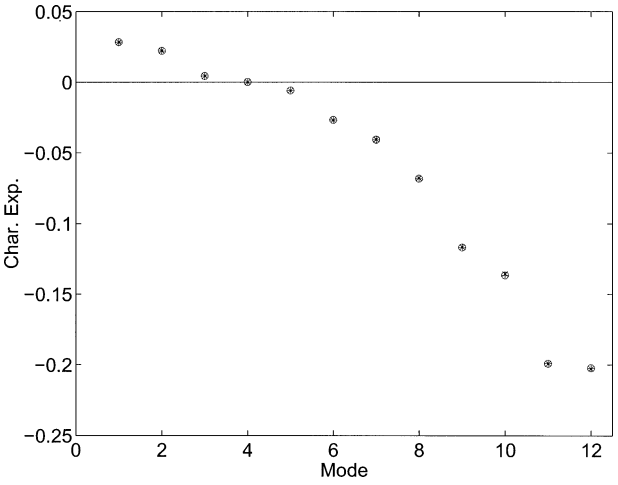

FIG. 3. Characteristic exponents vs mode number for the first 12 leading Floquet vectors. Four different values are shown for each exponent, corresponding to different approximations to the full Floquet problem with truncations to 120 (·), 264 (○), 240 (×), and 528 (+) independent initial disturbances and resulting eigenvectors, respectively.

Modes 1–3, the unstable modes, have a broadly similar structure, but differ in significant ways. The amplitudes $|\Phi^j|$ of all three of these oscillate markedly, and essentially in phase with the amplitude of the wave-mean cycle: they reach maximum values near $t/T = 13/50$, when the wave-mean-cycle wave amplitude is maximum (Figs. 5–7). All three are dominated by low-wavenumber Fourier components. Mode 2, like the wave-mean cycle and mode 4, is dominated by the gravest along-channel and across-channel Fourier component (Fig. 6), while modes 1 and 3 show large contributions from the second along-channel Fourier component (Figs. 5–7). This difference means that the instability represented by mode 2 involves either an intensification or weakening, depending on the sign of the disturbance, of the entire wave-mean cycle, while the instabilities represented by modes 1 and 3 involve an asymmetric development, in which the high pressure centers intensify and the low pressure centers weaken, or the lows intensify and the highs weaken. These differences are especially apparent in the thermal streamfunctions ψ_T^j, with ψ_T^2 (and of course ψ_T^4) generally resembling Ψ_T, and ψ_T^1 and ψ_T^3 having qualitatively different spatial symmetries.

The structure function Φ^2 for mode 2 has a very similar structure and evolution to Φ^4, the neutral mode. There are weakly damped modes that closely resemble the other two growing modes also: Φ^6 is similar to Φ^3, and Φ^7 to Φ^1 (Figs. 8 and 9). This illustrates that relatively small changes in disturbance structure are sufficient to control stability. This similarity of growing and neutral or decaying modes will have implications for the calculation of optimal disturbances.

Among the first seven modes, the weakly damped mode 5 stands out as most unlike any other. It has two isolated, roughly barotropic extrema in streamfunction,

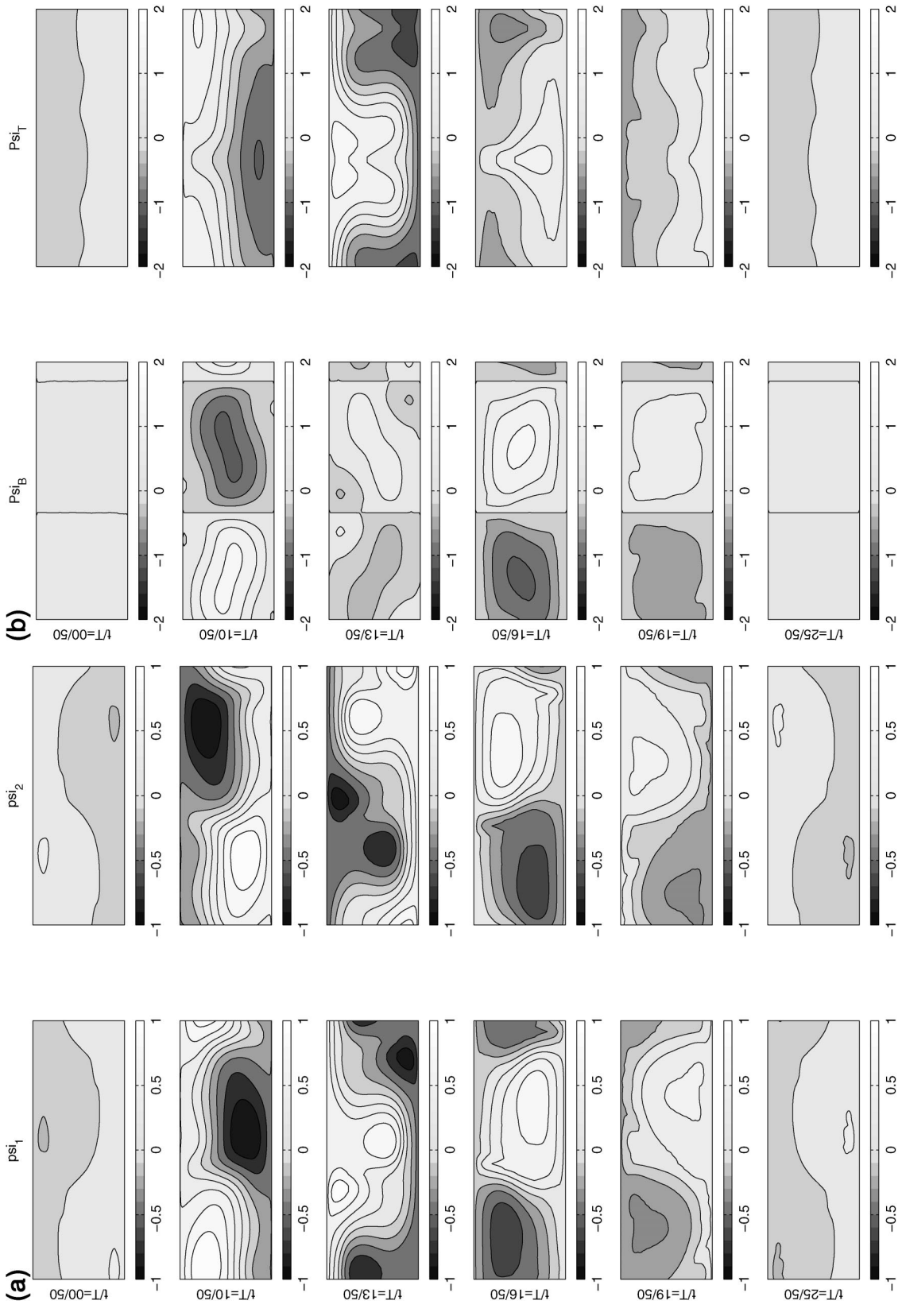

FIG. 4. (a) Contours of upper- (lhs) and lower-layer (rhs) streamfunctions vs x (horizontal axes) and y (vertical axes) for the structure function Φ^4 of the fourth, neutral Floquet vector during the evolution of the wave-mean oscillation. (b) Contours of barotropic (lhs) and baroclinic (rhs) streamfunctions vs x (horizontal axes) and y (vertical axes) for the structure function Φ^4 of the fourth neutral Floquet vector during the evolution of the wave-mean oscillation.

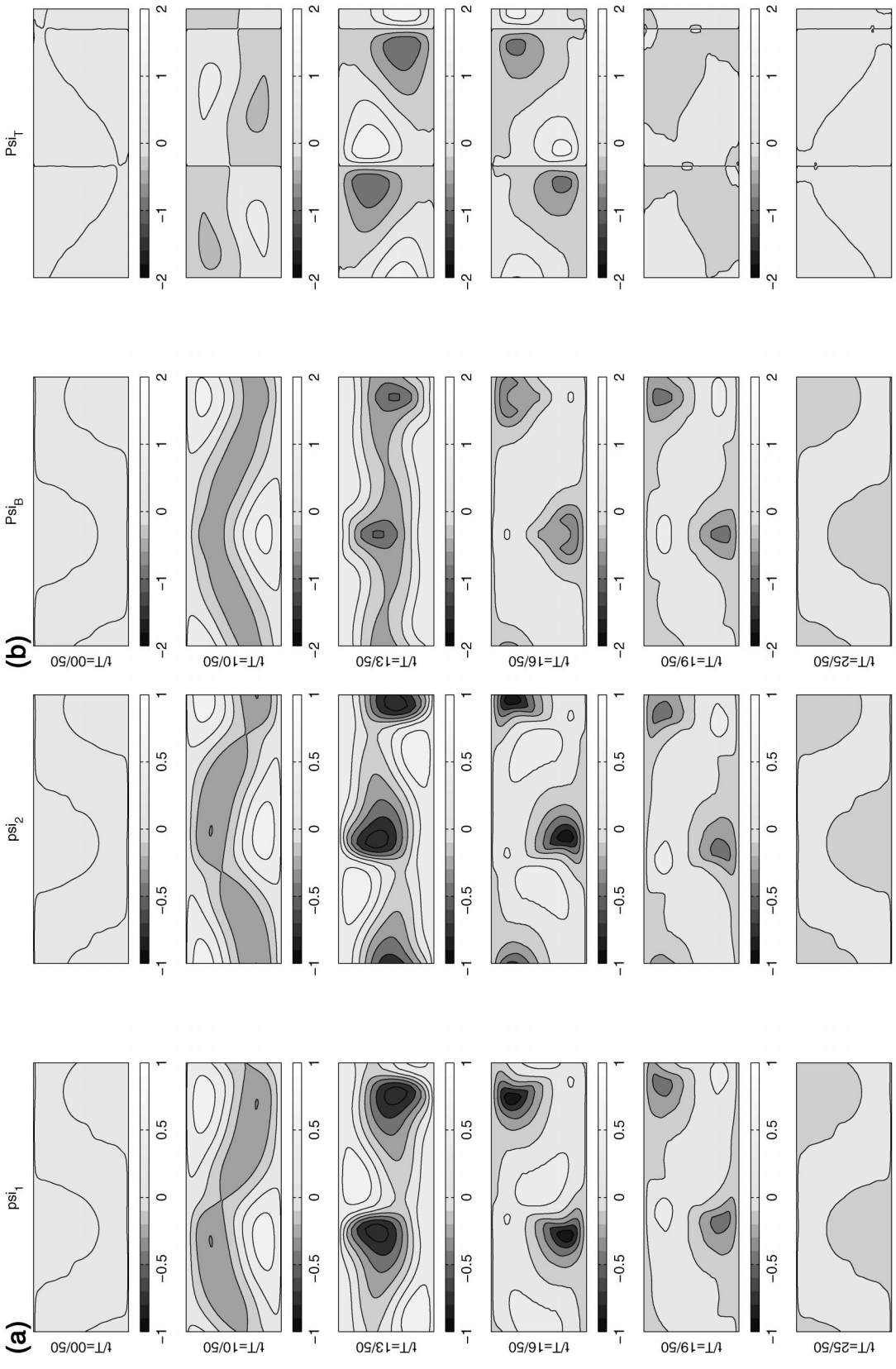

FIG. 5. (a) Contours of upper- (lhs) and lower-layer (rhs) streamfunctions vs x (horizontal axes) and y (vertical axes) for the structure function Φ^1 of the leading Floquet vector during the evolution of the wave-mean oscillation. (b) Contours of barotropic (lhs) and baroclinic (rhs) streamfunctions vs x (horizontal axes) and y (vertical axes) for the structure function Φ^1 of the leading Floquet vector during the evolution of the wave-mean oscillation.

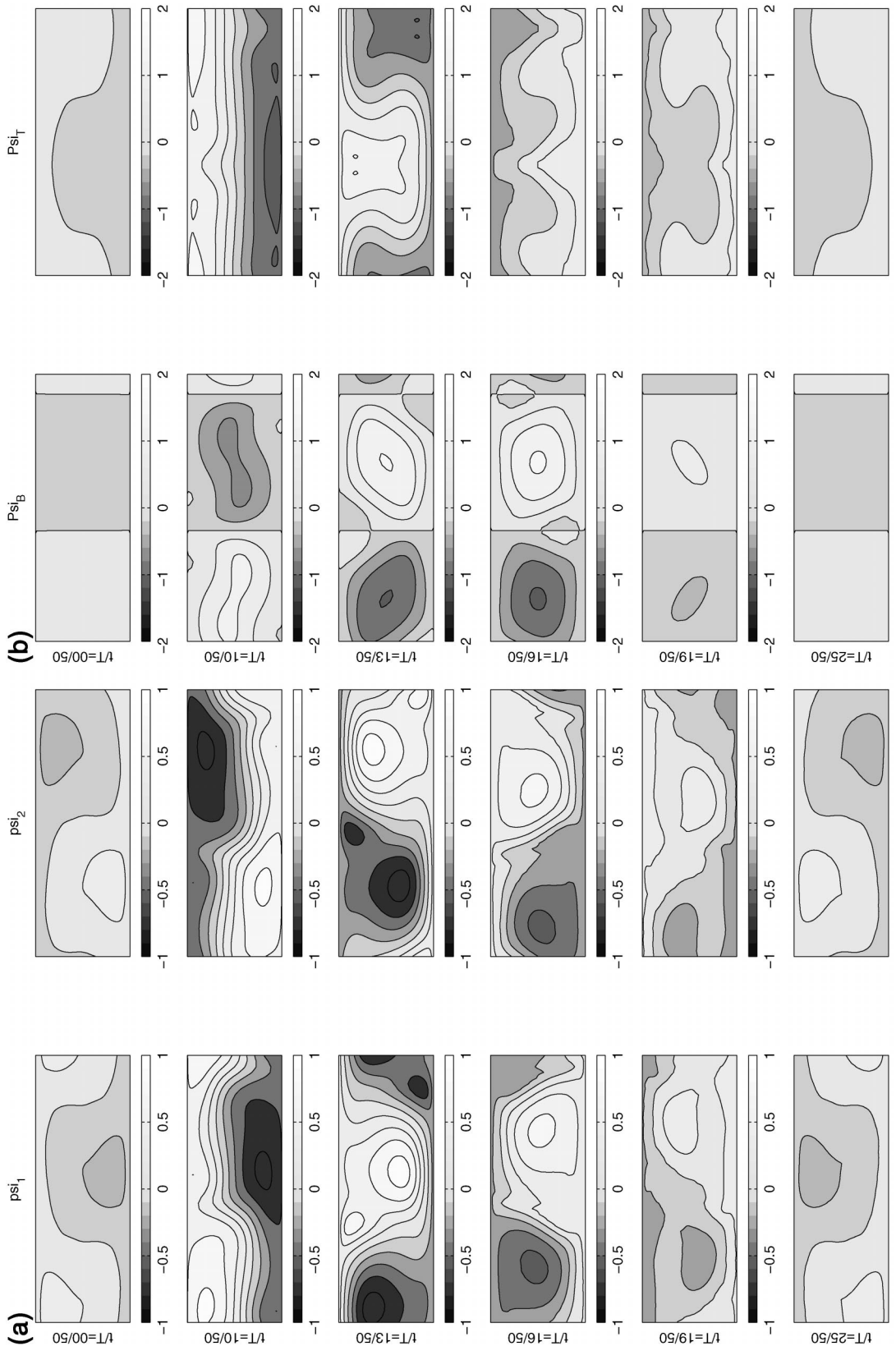

FIG. 6. (a) Contours of upper- (lhs) and lower-layer (rhs) streamfunctions vs x (horizontal axes) and y (vertical axes) for the structure function Φ^2 of the second Floquet vector during the evolution of the wave-mean oscillation. (b) Contours of barotropic (lhs) and baroclinic (rhs) streamfunctions vs x (horizontal axes) and y (vertical axes) for the structure function Φ^2 of the second Floquet vector during the evolution of the wave-mean oscillation.

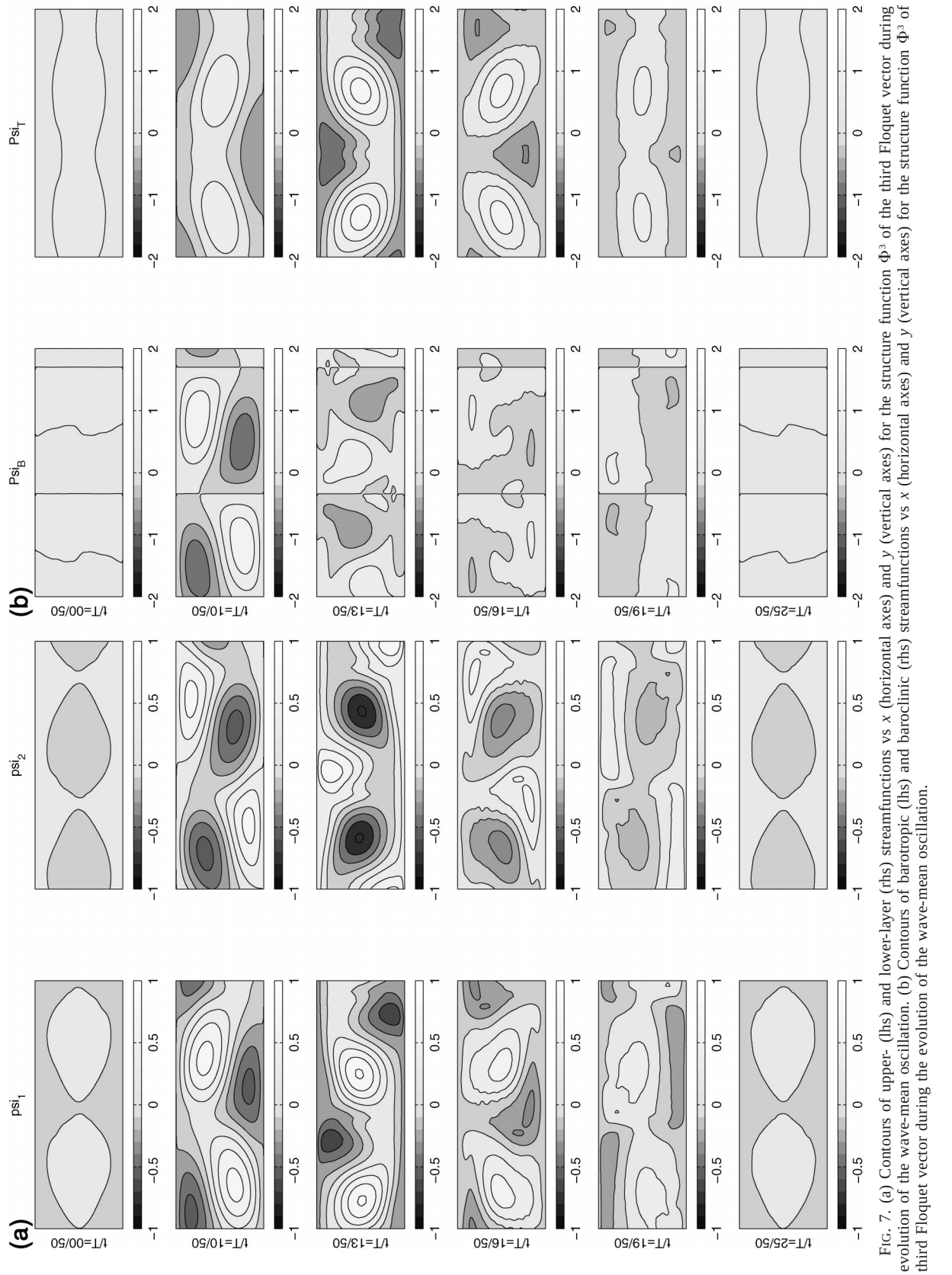

FIG. 7. (a) Contours of upper- (lhs) and lower-layer (rhs) streamfunctions vs x (horizontal axes) and y (vertical axes) for the structure function Φ^3 of the third Floquet vector during the evolution of the wave-mean oscillation. (b) Contours of barotropic (lhs) and baroclinic (rhs) streamfunctions vs x (horizontal axes) and y (vertical axes) for the structure function Φ^3 of the third Floquet vector during the evolution of the wave-mean oscillation.

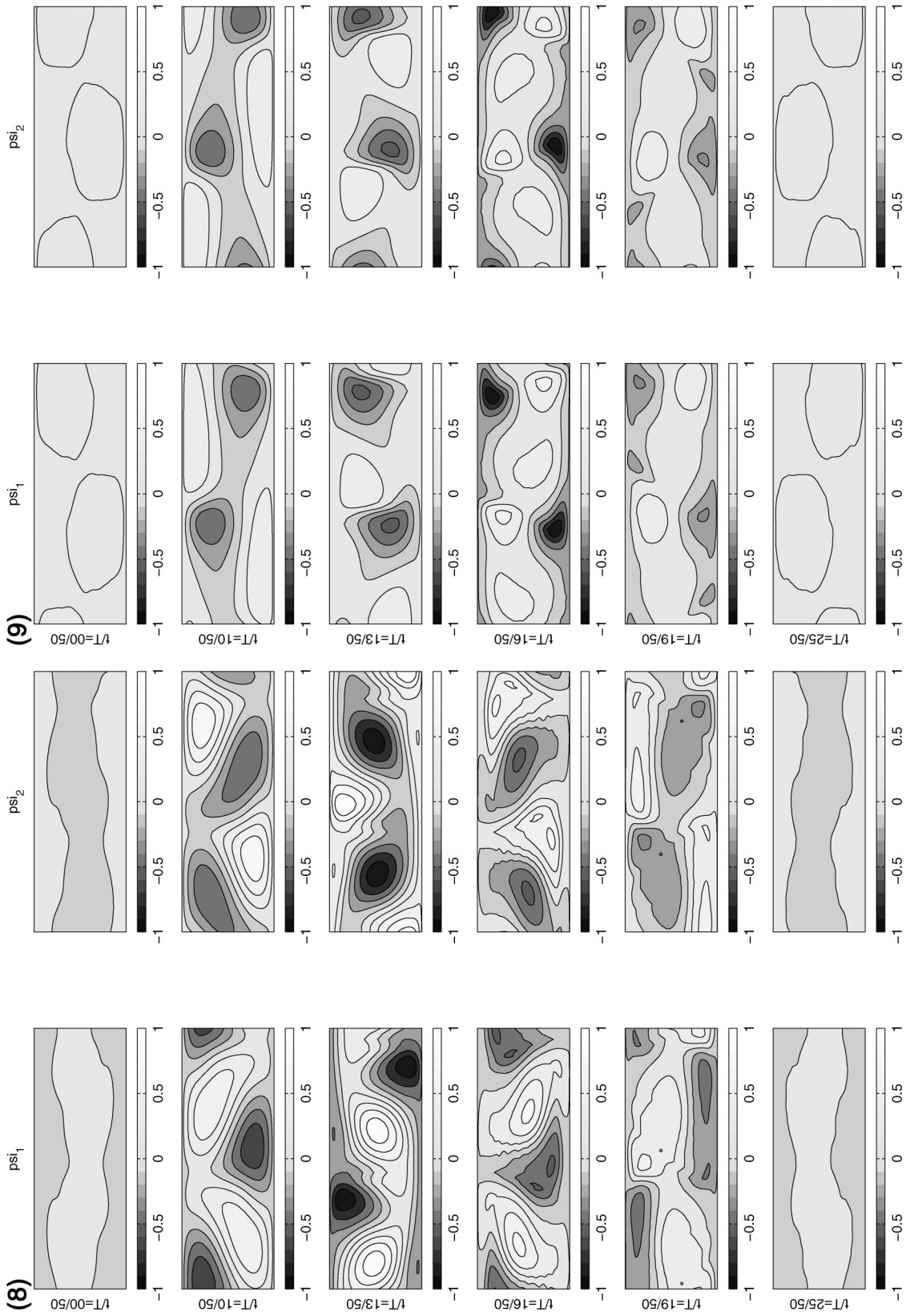

FIG. 8. Contours of upper- (lhs) and lower-layer (rhs) streamfunctions vs x (horizontal axes) and y (vertical axes) for the structure function Φ^6 of the sixth decaying Floquet vector during the evolution of the wave-mean oscillation.

FIG. 9. Contours of upper- (lhs) and lower-layer (rhs) streamfunctions vs x (horizontal axes) and y (vertical axes) for the structure function Φ^7 of the seventh decaying Floquet vector during the evolution of the wave-mean oscillation.

located between the wave-mean-cycle streamfunction extrema, and evidently represents, in part, an along-channel phase shift of the entire cycle (Fig. 10). As can be verified by visual inspection, mode 5 is approximately proportional to the along-channel gradient of the wave-mean oscillation at each fixed time.

Some of the higher, more rapidly damped modes, such as mode 12 (Fig. 11), have much smaller spatial scales. The amplitudes of these modes typically oscillate much less during the course of the wave-mean cycle, representing instead a disturbance with roughly uniform instantaneous decay rate. Animations of these modes show that the smaller-scale features are advected rapidly along the channel and around the pressure centers by the time-dependent velocity field of the wave-mean cycle. Because of their relatively small horizontal scales, the upper- and lower-layer features are not strongly coupled vertically, and are often advected in opposite directions in the two layers.

The existence of multiple growing normal modes on the wave-mean cycle is evidently related to the existence of multiple growing normal modes on the underlying steady parallel zonal flow. The dominant spatial structure of the three growing Floquet modes corresponds, respectively, to the spatial structure of the three leading normal modes of the underlying steady parallel flow (Klein and Pedlosky 1986, Table 1): both occur in the order (2,1), (1,1), (2,2), where the pairs (k, m) indicate the kth along-channel and mth cross-channel Fourier components. However, the wave-mean cycle is much less unstable than the underlying steady parallel flow: the growth rates of the leading Floquet modes are more than an order of magnitude smaller than those of the leading normal modes of the steady flow. This near-stabilization is evidently due primarily to a reduction in the mean vertical shear of the zonal flow, relative to the undisturbed value $U_s = 1$. The time- and along-channel mean, during one cycle of the wave-mean oscillation, of the vertical shear of the zonal flow is 0.126 at the center of the channel, less than the critical value of 0.14, and 0.179 when averaged across the central half of the channel width. Note that the oscillation is sufficiently nonlinear that the sign of the mean along-channel vertical shear in the central part of the channel reverses when the wave amplitude is maximum (Fig. 2a).

Floquet eigenvalues for many higher modes were also obtained from the first Newton–Picard method. These estimates appeared to be relatively reliable and independent of the truncation level, despite the difficulties presented by the more delicate reconstruction of the corresponding damped Floquet modes themselves. These had a distribution similar to that of the normal mode growth rates for the steady flow and for the weakly nonlinear oscillation treated by Samelson (2001): a small number of growing or weakly damped modes, a similar small number of rapidly damped modes, and a large number of intermediate modes with damping rate close to the value of the friction parameter r. Some broadening of the spectrum of the growing or weakly damped modes was observed for the nonlinear cycle, however, as roughly 20 of the Floquet modes fell into this class, compared to only 10 of the steady flow normal modes.

Samelson (2001) found that the most rapidly decaying mode in the weakly nonlinear case was inviscidly damped, with phase shift opposite to that appropriate for a growing baroclinic disturbance, analogous to the complex conjugate of the growing mode in the steady parallel flow. In the present case, reliable estimates of the spatial structure of the most rapidly decaying modes were not available, and it was therefore not possible to determine whether similar inviscidly damped modes existed. However, the similarity of the structure of the eigenvalue spectrum to the weakly nonlinear and steady flow results suggests that such inviscidly damped modes exist also in the present case.

5. Summary

The primary achievement of this study is the identification, in a 3840-dimensional numerical model, of a strongly nonlinear baroclinic wave-mean oscillation that is linearly unstable to multiple normal mode disturbances. Accurate numerical solutions for this cycle were obtained by two different Newton–Picard methods, the first using direct estimates of a large number of Floquet vectors, and the second using the efficient iterative solver developed by Lust et al. (1998). This unstable cycle is one among many that presumably exist in any chaotic regime of these equations. Analysis of its leading Floquet vectors illustrated that, as in the weakly nonlinear case studied by Samelson (2001, 2002), disturbance growth and decay on the wave timescale are dominated by baroclinic wave growth and decay processes similar to those that give rise to the wave-mean oscillation.

These results illustrate that Newton–Picard methods can be used effectively to compute an unstable cycle in a strongly nonlinear, high-dimensional geophysical fluid dynamics model. Such cycles will provide valuable physical examples in which the the mechanisms and properties of disturbance growth in unstable time-dependent flows can be analyzed in detail. In addition to their value as theoretical examples, it seems likely that future insights resulting from the analysis of flows of this type will have practical value for the analysis and development of ensemble forecasting schemes in numerical weather prediction.

Although the present model has a relatively confined geometry, and an underlying steady parallel zonal flow that is unstable at only a few zonal wavenumbers, it may well be possible to find similar, highly symmetric oscillatory solutions in models with extended domains. For example, consider extending the present model to a larger zonal domain by patching several copies of the model channel together at their ends. Because it is also zonally periodic, the present solution will extend exactly

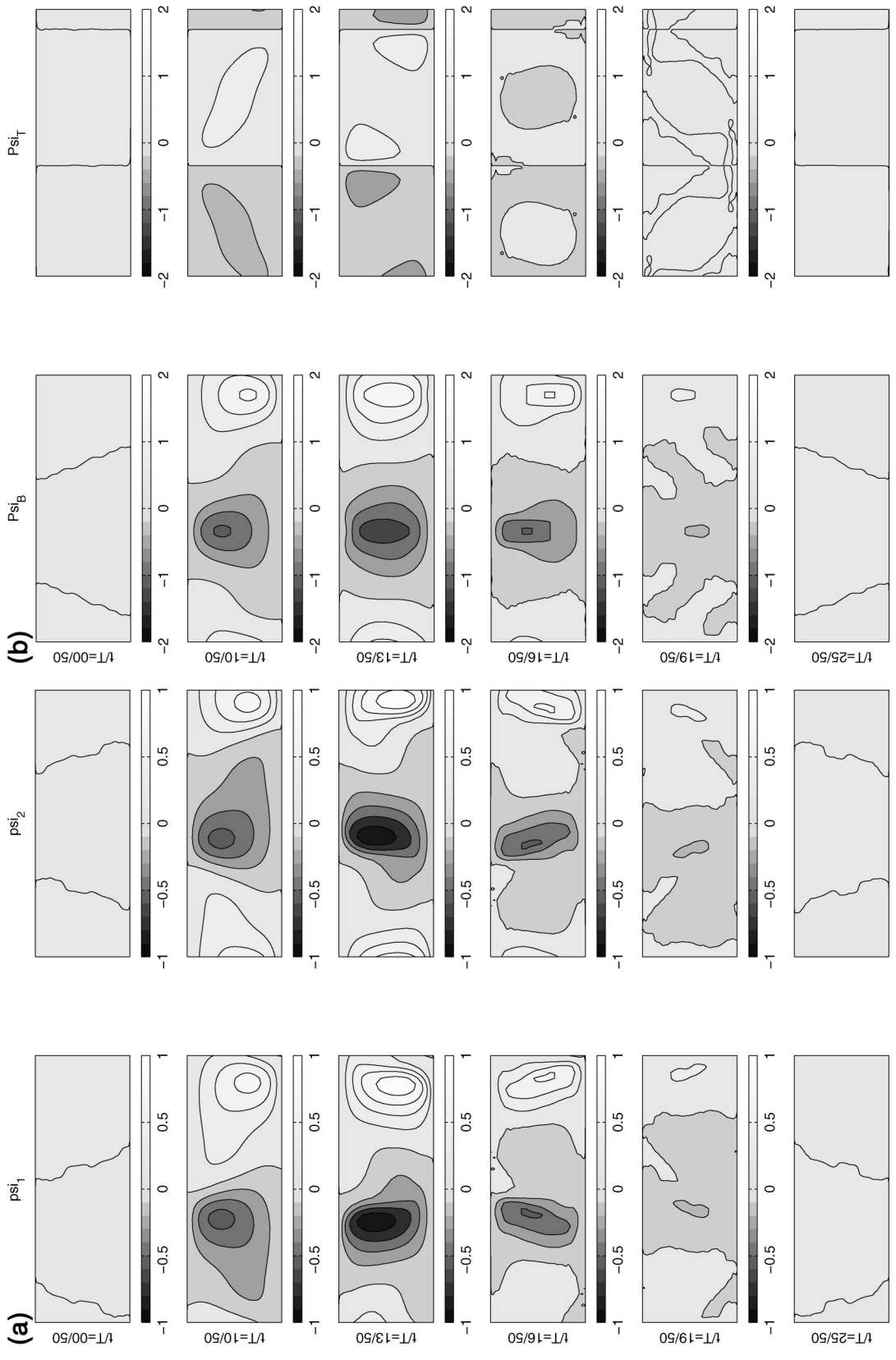

FIG. 10. (a) Contours of upper- (lhs) and lower-layer (rhs) streamfunctions vs x (horizontal axes) and y (vertical axes) for the structure function Φ^5 of the fifth decaying Floquet vector during the evolution of the wave-mean oscillation. (b) Contours of barotropic (lhs) and baroclinic (rhs) streamfunctions vs x (horizontal axes) and y (vertical axes) for the structure function Φ^5 of the fifth, decaying Floquet vector during the evolution of the wave-mean oscillation.

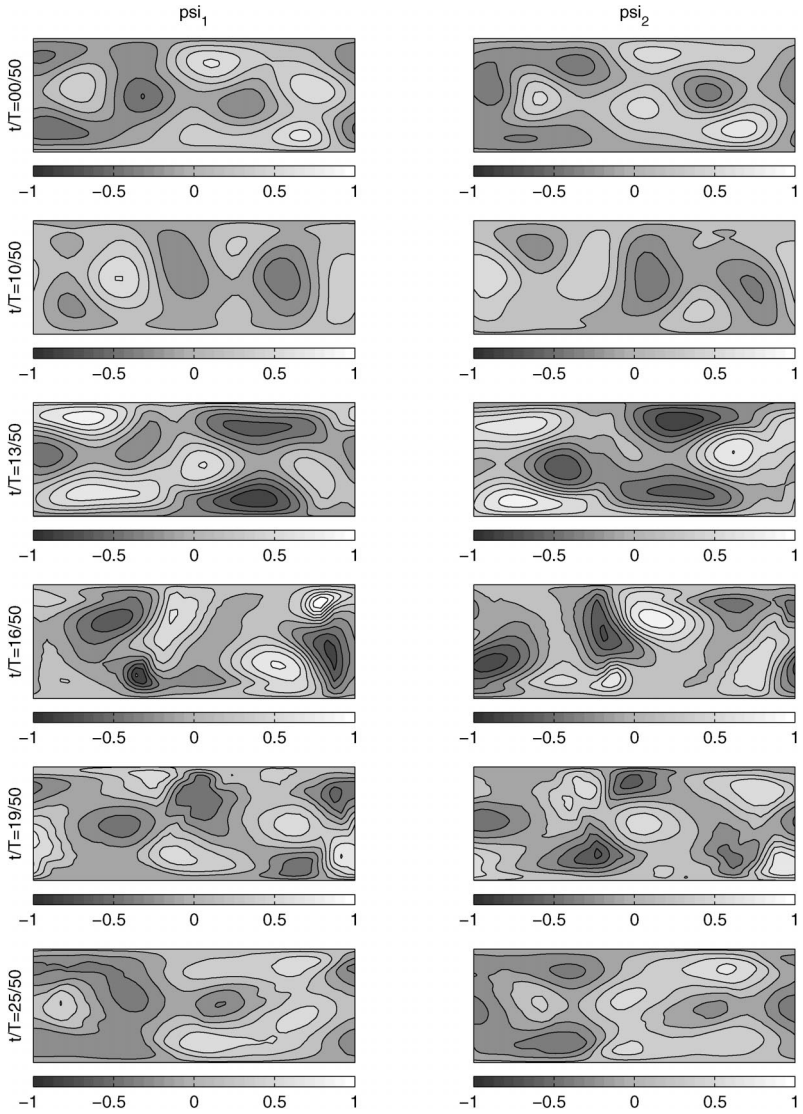

FIG. 11. Contours of upper- (lhs) and lower-layer (rhs) streamfunctions vs x (horizontal axes) and y (vertical axes) for the structure function Φ^{12} of the twelfth decaying Floquet vector during the evolution of the wave-mean oscillation.

to a time-periodic solution in the larger domain, despite the possibility of additional instabilities with larger zonal wavelengths, and the present Floquet eigenmodes will remain eigenmodes of this extended solution. Presumably, less trivial analogs will also exist.

Acknowledgments. This research was supported by the Office of Naval Research, Grant N00014-98-1-0813, Code 322 OM. We are grateful to K. Lust for providing the PDECONT software to us.

REFERENCES

Benettin, G., L. Galgani, A. Giorgilli, and J.-M. Strelcyn, 1980: Lyapunov characteristic exponents for smooth dynamical systems and for Hamiltonian systems: A method for computing all of them. Part I: Theory. *Meccanica,* **15,** 9–20.

Brevdo, L., and T. J. Bridges, 1997: Local and global instabilities of spatially developing flows: Cautionary examples. *Proc. Roy. Soc. London,* **A453,** 1345–1364.

Charney, J., 1947: The dynamics of long waves in a baroclinic westerly current. *J. Meteor.,* **4,** 135–162.

Coddington, E., and N. Levinson, 1955: *Theory of Ordinary Differential Equations.* McGraw-Hill, 429 pp.

Eady, E., 1949: Long waves and cyclone waves. *Tellus,* **1,** 33–52.

Fantini, M., and S. Davolio, 2001: Instability of neutral Eady waves and orography. *J. Atmos. Sci.,* **58,** 1146–1154.

Farrell, B., and P. Ioannou, 1996: Generalized stability theory. Part I: Autonomous operators. *J. Atmos. Sci.,* **53,** 2025–2040.

Itoh, H., and M. Kimoto, 1996: Multiple attractors and chaotic itinerancy in a quasigeostrophic model with realistic topography: Implications for weather regimes and low-frequency variability. *J. Atmos. Sci.,* **53,** 2217–2231.

Jiang, S., and M. Ghil, 1997: Tracking nonlinear solutions with simulated altimetric data in a shallow-water model. *J. Phys. Oceanogr.*, **27,** 72–95.

——, F. Jin, and M. Ghil, 1995: Multiple equilibria, periodic and aperiodic solutions in a wind-driven double-gyre shallow-water model. *J. Phys. Oceanogr.*, **25,** 764–785.

Joly, A., and A. Thorpe, 1991: The stability of time-dependent flows: An application to fronts in developing baroclinic waves. *J. Atmos. Sci.*, **48,** 163–182.

Kazantsev, E., 1998: Unstable periodic orbits and attractor of the barotropic ocean model. *Nonlinear Processes Geophys.*, **5,** 193–208.

——, 2001: Sensitivity of the attractor of the barotropic ocean model to external influences: Approach by unstable periodic orbits. *Nonlinear Processes Geophys.*, **8,** 281–300.

Klein, P., and J. Pedlosky, 1986: A numerical study of baroclinic instability at large supercriticality. *J. Atmos. Sci.*, **43,** 1243–1262.

Lust, K., D. Roose, A. Spence, and A. Champneys, 1998: An adaptive Newton–Picard algorithm with subspace iteration for computing periodic solutions. *SIAM J. Sci. Comp.*, **19,** 1188–1209.

Pedlosky, J., 1971: Finite-amplitude baroclinic waves with small dissipation. *J. Atmos. Sci.*, **28,** 587–597.

——, and C. Frenzen, 1980: Chaotic and periodic behavior of finite-amplitude baroclinic waves. *J. Atmos. Sci.*, **37,** 1177–1196.

Phillips, N., 1954: Energy transformations and meridional circulations associated with simple baroclinic waves in a two-level, quasi-geostrophic model. *Tellus*, **6,** 273–286.

Samelson, R. M., 2001: Periodic orbits and disturbance growth for baroclinic waves. *J. Atmos. Sci.*, **58,** 436–450.

——, 2002: Lyapunov, Floquet, and singular vectors for baroclinic waves. *Nonlinear Processes Geophys.*, **8,** 439–448.

——, and J. Pedlosky, 1990: Local baroclinic instability of flow over variable topography. *J. Fluid Mech.*, **221,** 411–436.

——, and E. Tziperman, 2001: Instability of the chaotic ENSO: The growth-phase predictability barrier. *J. Atmos. Sci.*, **58,** 3613–3625.

Shimada, I., and T. Nagashima, 1979: A numerical approach to ergodic problem of dissipative dynamical systems. *Prog. Theor. Phys.*, **61,** 1605–1616.